minerals

MDPI

Article

On the Chemical Composition and Possible Origin of Na–Cr-Rich Clinopyroxene in Silicocarbonatites from Samalpatti, Tamil Nadu, South India

Ondřej Krátký [1,2,3,*], Vladislav Rapprich [1], Martin Racek [2], Jitka Míková [1] and Tomáš Magna [1]

[1] Czech Geological Survey, Klárov 3, CZ-118 21 Prague 1, Czech Republic; vladislav.rapprich@geology.cz (V.R.); jitka.mikova@geology.cz (J.M.); tomas.magna@geology.cz (T.M.)
[2] Faculty of Science, Charles University in Prague, Albertov 6, CZ-128 43 Prague 2, Czech Republic; martin.racek2@gmail.com
[3] Faculty of Science, Masaryk University, Kotlářská 2, CZ-602 00 Brno, Czech Republic
* Correspondence: ondra.kratky@gmail.com

Received: 26 June 2018; Accepted: 11 August 2018; Published: 17 August 2018

Abstract: Mineralogical and chemical data are presented for a suite of Na–Cr-rich clinopyroxenes associated with chromite, winchite (sodium-calcium amphibole), titanite and calcite in Mg-Cr-rich silicocarbonatites from the Samalpatti carbonatite complex, Tamil Nadu, South India. The Mg-Cr-rich silicocarbonatites occur as 10–30 cm large enclaves in pyroxenites. The chemical composition of the pyroxenes differs among individual enclaves, with variable proportions of diopside, kosmochlor and jadeite-aegirine end-members. These compositions fill a previously unoccupied space in the kosmochlor-diopside-jadeite+aegirine ternary plot, indicating a distinct origin of kosmochlor-rich pyroxene compared with previous findings from diverse settings. The Na–Cr-rich clinopyroxene has low ΣREE = 9.2 ppm, with slight enrichment in LREE (La_N = 7), coupled with low HREE (Yb_N = 0.6), and flat HREE, paralleled by a significant fractionation of Nb/Ta (2408) and Th/U (26.5). Sodic metasomatism (fenitization) associated with either carbonatite emplacement at shallow levels or during carbonatite ascent through the upper mantle most likely was the major process operating in the area. We suggest two scenarios of the formation of Na–Cr-rich pyroxene: (1) from mantle-derived chromian mineral phases (spinel and/or garnet) through fenitization, with subsequent corrosion by growing winchite due to volatile influx; (2) via metasomatic reaction of Cr-rich garnet in mantle peridotite due to reaction with Na-rich carbonatite melt. Collectively, the appearance of kosmochlor may play an important role in deconvolving metasomatic processes, and fenitization in particular. If combined with petrologic experiments, it could improve our understanding of the origin and subsequent history of chemical signatures of carbonate-rich materials in the mantle.

Keywords: Na–Cr-rich pyroxene; kosmochlor; chromite; sodic metasomatism; silicocarbonatite; mineral chemistry; Samalpatti carbonatite complex

1. Introduction

Chromium enters the crystal structure of pyroxenes in variable amounts. Only small admixtures of Cr can be found in common calcic clinopyroxenes with a structural formula $M2M1(Si,Al)_2O_6$, where M2 site is occupied mainly by Na and Ca, and M1 site by Mg, Fe^{2+}, Al, V, Ti, Fe^{3+} and Cr^{3+}, respectively. On the other hand, Cr plays a more important role in the structure of sodic clinopyroxenes, where kosmochlor/ureyite ($NaCrSi_2O_6$) is a chromian end-member of this group. The other two end members are jadeite ($NaAlSi_2O_6$) + aegirine ($NaFeSi_2O_6$) [1] and diopside ($MgCaSi_2O_6$), and kosmochlor forms a solid solution with each of these. Reznitsky et al. [2] found

that pyroxenes from kimberlites are very rich in chromium and have up to 42 mol % of kosmochlor component. They also stated that pyroxenes from kimberlites do not fall close to the most common diopside–kosmochlor binary join and that, as a consequence, these pyroxenes contain other components (aegirine, jadeite) in tens of mol %. Also, in their study, a complete isomorphic diopside–kosmochlor join was identified for the first time in the nature (Sludyanka compley, Baikal region, Russia). The simple binary diopside–kosmochlor solid solution is more typical of meteorite pyroxenes and pyroxenes from granulites.

Thus far, kosmochlor was observed in only a limited range of natural occurrences. It was originally described as an accessory mineral in Toluca iron octahedrite [3] and other meteorites [4–6]. Furthermore, kosmochlor may be an important component in pyroxene grains of cometary dust e.g., [7–9]. It was also found in a limited number of terrestrial environments, mainly in high-grade metamorphic rocks such as jadeitites and associated rocks from Myanmar, Guatemala, and China [10–12], peridotite xenoliths [13] and granulites [2,14]. Chromium-rich pyroxenes were rarely also described from compositionally exotic mantle-derived magmatic rocks like kimberlites [15] and silicocarbonatites [16]. Laboratory experiments to synthesize kosmochlor and other Cr-rich pyroxenes produced a broad range of compositions (see [2] for more details) which is similar to that observed in nature, but there is still a lot of controversy between laboratory results and natural samples. A wide compositional range and specific conditions of occurrence make Na–Cr-rich pyroxene a possibly good candidate for further petrogenetic studies although this theoretical expectation requires thorough experimental work. These studies may also include distinguishing between high-grade metamorphic, primary magmatic, and post-magmatic metasomatic origin of unusual ultramafic rocks.

Here, we focus on detailed chemical composition of rare Na–Cr-rich pyroxene from silicocarbonatite nodules enclosed in pyroxenites of the Samalpatti carbonatite-alkaline silicate complex, Tamil Nadu, South India, and possible interpretation of its origin with respect to the geochemistry and petrogenesis of the Samalpatti complex. We anticipate that all studied "kosmochlor" grains will be termed here "Na–Cr-rich pyroxene" because the studied grains have a wide compositional range and majority of them contains less than 33 mol % of kosmochlor end-member in the ternary diagram. However, the rarity of such mineral compositions in nature encouraged us to a dedicated study with some first-order implications for their origin.

2. Geological Setting

The Samalpatti complex (700 ± 30 Ma; Moralev et al. [17]) belongs to a NE-SW trending belt of syenite, pyroxenite, dunite and carbonatite occurrences in the northern part of Tamil Nadu, south India [18,19], following the Koratti and Attur fault/shear zones [20,21]. The Samalpatti complex itself (>125 km^2; [19,22]) comprises syenites, carbonatites, silicocarbonatites, pyroxenites, alkali gabbros and serpentinized dunites, which intruded into hornblende-epidote gneisses (Figure 1). The complex has a large central syenite body surrounded by a discontinuous ring of pyroxenites. The calciocarbonatites and silicocarbonatites usually occur as elongated bodies, lenses and dykes or clusters of disseminated ~10–30 cm-sized enclaves in pyroxenites (Figures 1 and 2) and syenites defining a discontinuous ring [16,21]. These enclaves consist of carbonate, Cr-rich amphibole with inclusions of chromite and Na–Cr-rich pyroxene [16]. The origin of the carbonatite-silicate rock association has been interpreted to result from the carbonate and silicate melt separation from a carbonated nephelinitic magma [21] although several alternatives were recently discussed [16].

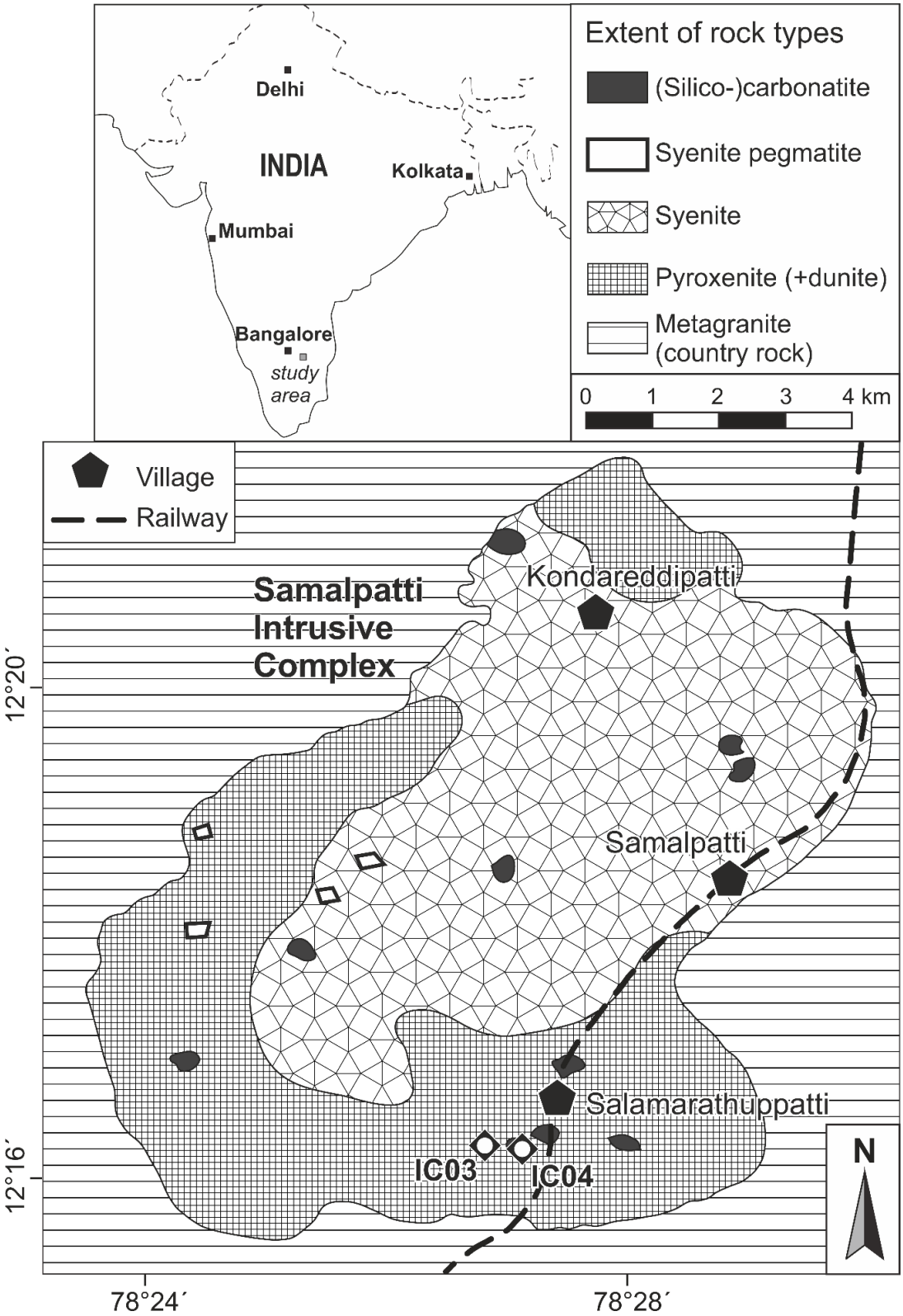

Figure 1. A simplified geological sketch of the Samalpatti carbonatite–alkaline silicate complex (after Schleicher et al. [23]; Srivastava [21]; Ackerman et al. [16]. Sampling sites are indicated.

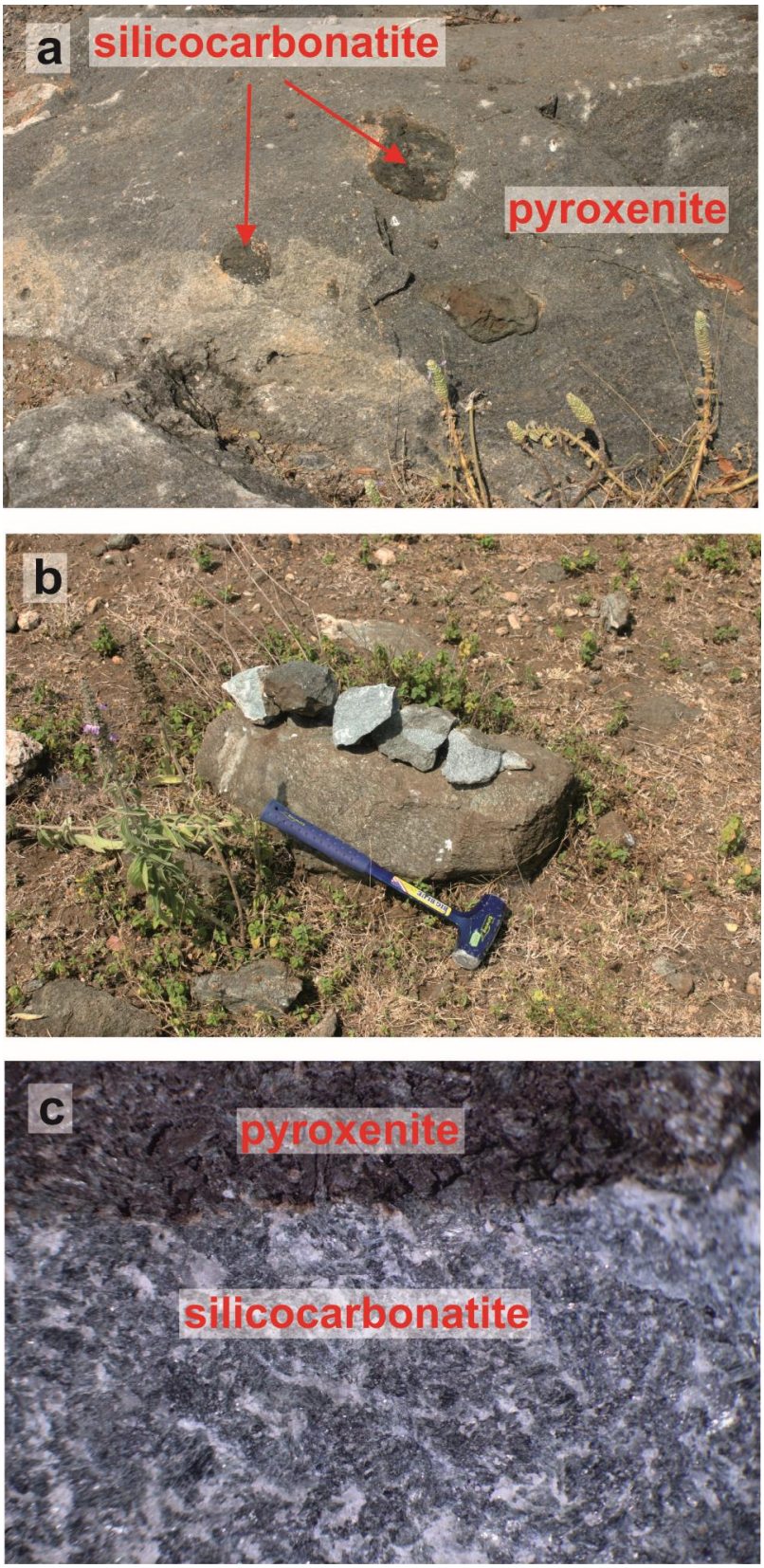

Figure 2. Occurrences of silicocarbonatite enclaves in pyroxenites of Samalpatti complex: (**a**) sampling site IC04, (**b**) sampling sit IC03, (**c**) detail of silicocarbonatite with hosting pyroxenite. Pictures (**b**,**c**) are adapted from Ackerman et al. [16].

3. Methods

Polished thin sections from seven Cr-rich silicocarbonatite enclaves from two outcrops of the Samalpatti complex were prepared at the Czech Geological Survey. The chemical composition of mineral phases was analyzed using a field emission gun electron probe micro-analyzer (FEG EPMA) JXA-8530F (Jeol Ltd., Akishima, Tokyo, Japan), housed at the Institute of Petrology and Structural Geology, Faculty of Science, Charles University (Prague, Czech Republic). The analyses were done with an accelerating voltage of 15 kV and beam current of 20 nA with the focused beam. Following standards (natural or synthetic materials) were used for the quantitative analyses: albite (Na), MgO (Mg), corundum (Al), quartz (Si), calcite (Ca), sanidine (K), rutile (Ti), Cr_2O_3 (Cr), rhodonite (Mn), magnetite (Fe). The method of Vieten and Hamm [24], which balances the deficiency of oxygen atoms corresponding to four cations (with all iron as Fe^{2+}), was used to calculate Fe^{3+} contents in clinopyroxenes. The same method based on three cations was applied to Fe–Cr oxides.

The concentrations of trace elements in Na–Cr-rich pyroxene as well as associated titanites and amphiboles were measured using an Analyte Excite 193 nm excimer-based laser ablation instrument (LA; Teledyne Photon Machines, Omaha, NE, USA) coupled with an Agilent 7900× ICPMS (Agilent Technologies, Santa Clara, CA, USA), housed at the Czech Geological Survey. Sample was ablated in He atmosphere (0.8 L/min), and the laser was fired at 5 Hz with a spot size of 20 μm and laser fluence of 7.59 J/cm^2. NIST 612 silicate glass wafer was used to monitor the accuracy and precision of the analyses. The raw data were processed using the Glitter software, developed by the ARC National Key Centre for Geochemical Evolution and Metallogeny of Continents (GEMOC) and CSIRO Exploration and Mining.

4. Results

4.1. Association and Crystal Shape

Sodium-Cr-rich pyroxene in samples IC03B and IC04A is mainly associated with chromite and titanite, and is enclosed in calcite and/or randomly oriented needles of sodium-calcium amphibole winchite [{CaNa}{Mg_4Al}(Si_8O_{22})$(OH)_2$] (Figure 3); minor plagioclase (pure albite), K-feldspar, and accessory apatite are also present. The Na–Cr-rich pyroxene grains have an irregular shape with residual crystals corroded by winchite or calcite (Figure 3a,b), and frequently contain inclusions of titanite (Figure 3c,d). Chromite forms either skeletal aggregates or individual grains in Na–Cr-rich pyroxene (Figure 3f). The maximum grain size of Na–Cr-rich pyroxene is ~0.2 mm but, in general, the size of Na–Cr-rich pyroxene grains is ~40 μm. Titanite is present as euhedral crystals up to ~80 μm in size. Back-scattered electron (BSE) images (Figure 3e,f) show intimate association of Na–Cr-rich pyroxene with chromite, implying possible cogenetic relation.

4.2. Mineral Chemistry

Table 1 lists representative analyses from each investigated thin section. Full analytical data set for the studied Na–Cr-rich pyroxenes is given in Supplementary Materials. The analyzed grains of Na–Cr-rich pyroxene show a complex compositional variation even within one sample (e.g., IC03F) with most grains clustering between Kos_{10} and Kos_{40} (Figure 4). The content of Cr_2O_3 varies between 2.2 and 14.6 wt %. The contents of Na_2O, FeO, CaO and MgO vary as a result of variable contents of different end-members in the Kos-Quad-Jd + Ae system (Figure 3a). Mostly, the analyzed samples do not overlap compositionally and form rather individual clusters (according to individual samples) despite the range of pyroxene end-member compositions for the entire suite.

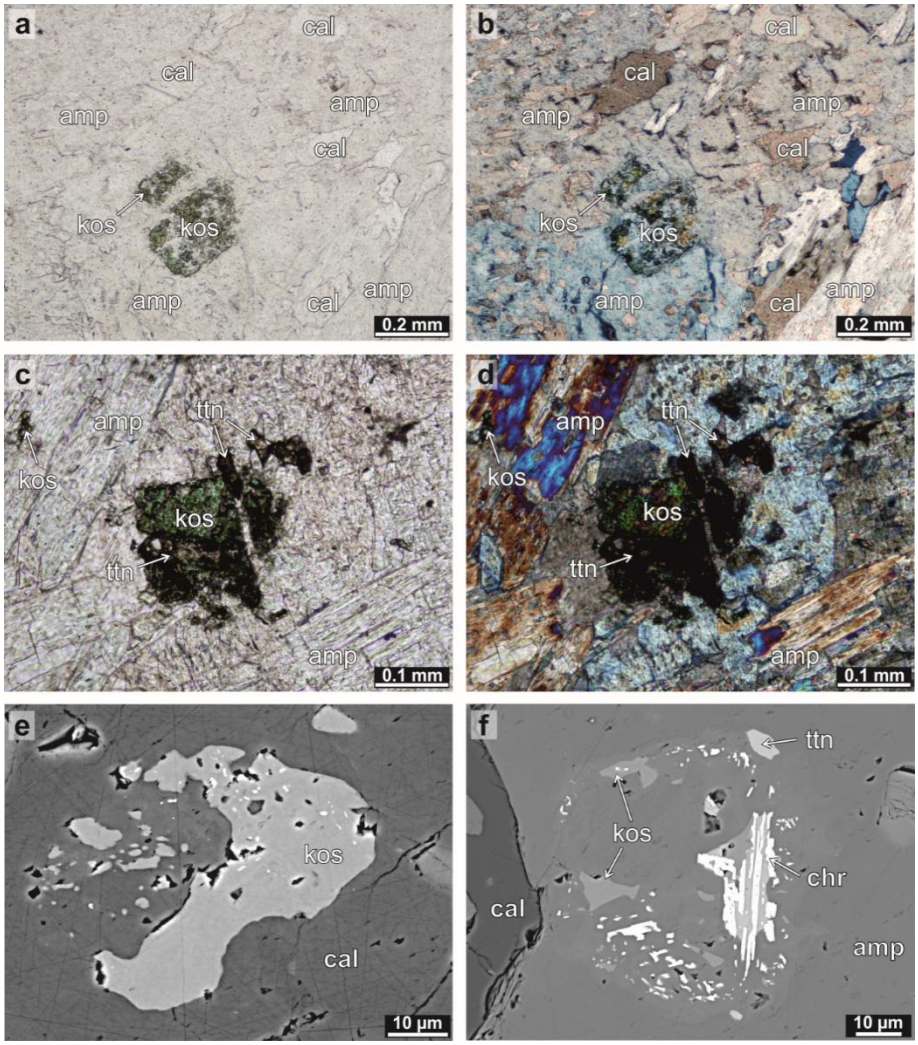

Figure 3. Microphotographs of Na–Cr-rich pyroxene in the investigated samples. Pictures on the left and right side are in plane-polarized and cross-polarized light, respectively. (**a**,**b**) Na–Cr-rich pyroxene grain from sample IC03D with amphibole and calcite. (**c**,**d**) Na–Cr-rich pyroxene grain from sample IC03E with associated titanite; (**e**) large Na–Cr-rich pyroxene grain from sample IC03B; (**f**) skeletal and partly decomposed grains of chromite with minor Na–Cr-rich pyroxene and titanite surrounded by amphibole in sample IC04A. For simplicity, Na–Cr-rich pyroxene is abbreviated 'kos' in this figure while we refer to the main text for further details on the chemistry of this phase. Mineral abbreviations after Whitney and Evans [25]: am—amphibole, cc—calcite, chr—chromite, kos—kosmochlor, ttn—titanite.

Table 1. Representative microprobe analyses and structural formulae of Na–Cr-rich pyroxenes from this study.

Sample		IC03B	IC03C	IC03D	IC03E	IC03F	IC03G	IC04A
Mineral Phase		Na–Cr–Px	Na–Cr–Px	Na–Cr–Px	Na–Cr–Px	Na–Cr–Px	Na–Cr–Px	Na–Cr–Px
SiO_2		53.69	52.56	53.53	52.72	53.44	54.15	53.75
TiO_2		0.41	0.40	4.61	0.20	0.30	0.21	0.26
Al_2O_3		0.8	0.89	1.05	1.03	1.09	1.02	0.82
Cr_2O_3		12.38	9.09	14.43	8.83	7.15	2.20	14.61
FeO		7.38	15.24	6.49	12.46	9.21	9.72	6.02
MnO		0.02	0.06	0.04	0.02	0.07	0.04	0.04
MgO		6.16	3.12	2.84	4.71	7.69	9.35	5.62
CaO		9.38	5.50	2.41	8.19	11.46	16.17	8.57
Na_2O		8.77	10.06	11.86	8.87	7.03	5.18	9.13
K_2O		0.00	0.00	0.00	0.00	0.00	0.00	0.00
Total		98.99	96.94	97.26	97.03	97.44	98.04	98.82
T	Si	2.00	2.02	2.04	2.02	2.02	2.03	2.01
M1	Al	0.04	0.04	0.05	0.05	0.05	0.05	0.04
	Ti	0.01	0.01	0.13	0.01	0.01	0.01	0.01
	Cr	0.37	0.28	0.44	0.27	0.21	0.07	0.43
	Fe^{3+}	0.20	0.37	0.05	0.30	0.19	0.20	0.15
	Mg	0.34	0.18	0.16	0.27	0.43	0.52	0.31
	Fe^{2+}	0.03	0.13	0.16	0.10	0.10	0.11	0.04
M2	Mn	0.00	0.00	0.00	0.00	0.00	0.00	0.00
	Ca	0.38	0.23	0.10	0.34	0.46	0.65	0.34
	Na	0.63	0.75	0.88	0.66	0.52	0.38	0.66

All data are in wt %. Structural chemical formulae in apfu (atoms per formula unit) based on 4 cations and 6 oxygens. The relatively low total is related to the high amount of ferric iron, analyzed as ferrous iron by the electron microprobe.

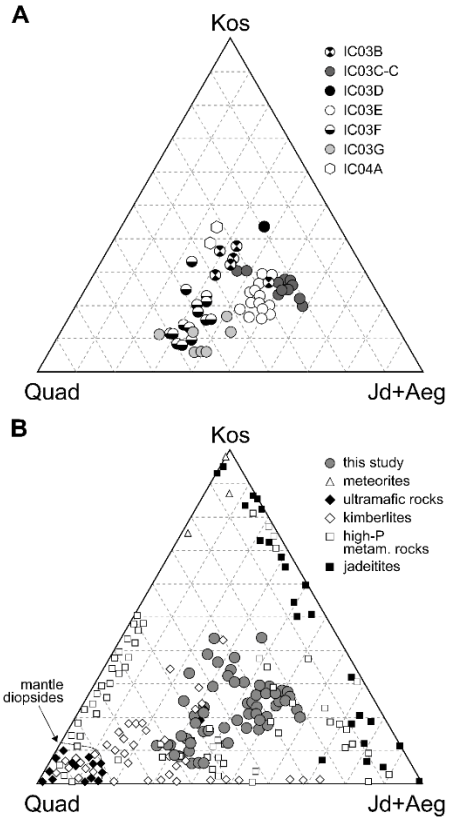

Figure 4. (**A**) Ternary diagram of Na–Cr-rich pyroxene grains from this study. (**B**) Ternary plot of data for Na–Cr-rich pyroxenes from this study and published compositions [15,26,27]. The published data also include kimberlite and peridotite xenoliths enclosed in basaltic host rocks. Quad represents sum of Ca + Fe + Mg pyroxenes [1].

Given the small size and corroded shape of Na–Cr-rich pyroxene grains, only one grain was suitable for the measurement of trace element concentrations using LA-ICPMS. The data is listed in Table 2 and chondrite-normalized REE abundances are plotted in Figure 5A. The Na–Cr-rich pyroxene has overall low contents of incompatible trace elements (ΣREE = 9.2 ppm) with a modest REE fractionation (La_N/Yb_N = 13.4) and a flat HREE pattern (Dy_N/Lu_N = 0.8). The REE pattern of Na–Cr-rich pyroxene is parallel to bulk-rock patterns of the pyroxenites and silicocarbonatites, though at lower REE concentrations. The Na–Cr-rich pyroxene also resembles the pyroxenites in the primitive mantle-normalized pattern of extended incompatible trace elements (Figure 5B). The only exception are the slightly higher abundances of HFSE (e.g., Ti = 6,134 ppm), with the exception of Ta, and Pb enrichment. Also, Th/U (26.5) and Nb/Ta (2408) fractionation is apparent, similar to titanite (Th/U 4.6–9.0 and Nb/Ta = 472–778, respectively). Unlike titanite, Zr–Hf is not depleted relative to neighboring elements (Figure 5B). Chromium content of ~118,500 ppm further supports elevated proportions of the non-chromian end-members in the investigated Na–Cr-rich pyroxene as determined from EMPA data because pure stoichiometric kosmochlor should have ~229,000 ppm Cr.

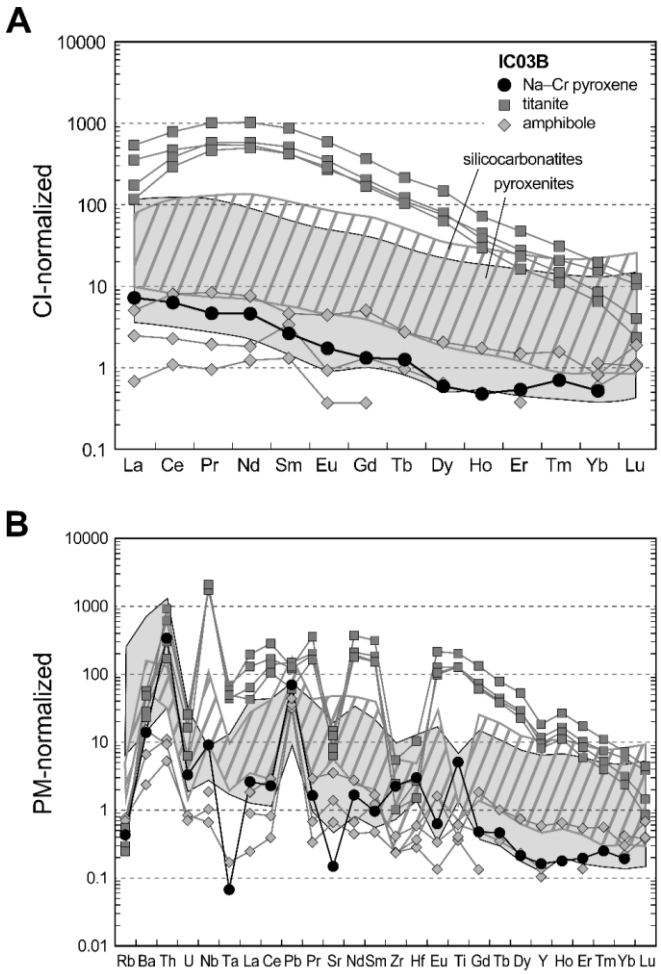

Figure 5. (**A**) Chondrite-normalized (Anders and Grevesse [28]) REE patterns of titanites, amphiboles and one Na–Cr-pyroxene grain from sample IC03B. Whole-rock data for the associated pyroxenites and silicocarbonatites [16] are also plotted; (**B**) Primitive mantle-normalized (McDonough and Sun [29]) multi-element concentrations in titanites, amphiboles and Na–Cr-pyroxene from IC03B. Both Na–Cr-rich pyroxene and titanite show similar features such as significant Nb–Ta fractionation and Sr depletion while Na–Cr-rich pyroxene shows extensive Pb enrichments and slight Zr–Hf enrichments (cf. Zr–Hf trough and Th enrichment in titanite). Ranges for host silicocarbonatites and pyroxenites [16] are also plotted for comparison.

Table 2. Trace element concentrations in sample IC03B analyzed by LA-ICPMS.

	Na–Cr-Rich Pyroxene	Titanite	Titanite	Titanite	Titanite	Amphibole	Amphibole	Amphibole
Li	12.0	8.91	bdl	bdl	bdl	bdl	8.80	bdl
Be	4.31	bdl	bdl	0.46	bdl	1.32	0.94	0.97
Sc	20.6	3.79	1.20	1.75	17.0	50.6	41.3	33.0
Ti	6134	155,064	151,645	154,576	243,407	434	731	489
V	239	112	53.1	20.6	303	92.5	52.6	48.4
Cr	118,478	832	847	837	14,510	3508	1703	2204
Co	52.4	3.89	0.85	2.27	15.6	55.0	38.3	28.8
Ni	48.0	26.8	5.38	10.7	86.0	284	178	151
Cu	1.43	1.53	0.85	0.54	1.95	2.10	2.28	2.36
Zn	2193	6.88	3.45	4.45	80.0	55.5	39.9	29.6
Ga	5.02	2.13	1.99	1.62	4.96	2.11	1.69	1.22
Rb	0.26	0.18	0.15	bdl	0.33	0.46	0.42	0.30
Sr	2.96	294	249	164	128	13.1	27.8	70.3
Y	0.70	50.7	41.1	35.1	78.6	0.45	0.59	2.53
Zr	23.6	25.8	10.6	10.6	57.1	2.51	4.36	2.47
Nb	6.02	1214	1261	1385	1137	0.43	1.23	0.68
Ba	91.4	376	319	191	153	15.7	44.0	101
La	1.70	83.7	41.1	27.6	126	0.16	0.58	1.19
Ce	3.83	284	231	176	474	0.66	1.38	4.83
Pr	0.42	48.7	51.8	41.6	90.6	0.085	0.17	0.75
Nd	2.09	244	264	225	464	0.56	0.83	3.43
Sm	0.39	62.3	75.3	61.9	128	0.19	0.50	0.68
Eu	0.097	15.1	19.5	16.2	33.3	0.021	0.052	0.25
Gd	0.26	35.5	40.2	33.1	71.9	0.073	0.26	1.00
Tb	0.046	4.02	4.43	3.80	7.77	bdl	0.035	0.10
Dy	0.14	18.1	19.5	15.3	35.9	bdl	0.16	0.50
Ho	0.027	2.49	2.11	1.65	4.00	bdl	bdl	0.097
Er	0.086	4.44	3.69	2.60	7.53	0.06	0.083	0.24
Tm	0.017	0.51	0.36	0.27	0.75	bdl	bdl	0.038
Yb	0.085	2.54	1.38	1.05	3.20	0.096	0.19	0.13
Lu	bdl	0.26	0.098	0.057	0.30	0.027	0.026	0.046
Hf	0.85	0.75	0.43	0.76	2.93	0.080	0.17	0.10
Ta	0.003	2.57	1.62	1.83	2.18	0.006	bdl	bdl
W	0.12	0.40	0.50	0.046	0.72	bdl	bdl	0.032
Pb	10.5	18.2	22.2	9.17	19.3	4.75	5.36	6.62
Th	6.91	12.4	6.09	3.48	18.8	0.11	0.22	0.19
U	0.26	1.95	1.31	0.50	2.08	0.067	bdl	0.056
ΣREE	9.19	805	754	607	1448	1.93	4.26	13.3

All concentrations are in ppm. bdl—below detection limit.

Sodium-Cr-rich pyroxene grains are mainly enclosed by winchite. Microprobe analyses show that winchite has low concentrations of Cr_2O_3, usually <0.5 wt %. Therefore, chromium for Na–Cr-rich clinopyroxene should be sourced from other mineral phases than winchite, also supported by petrographic evidence for late origin of winchite relative to Na–Cr-rich pyroxene. Amphiboles have REE and incompatible trace element patterns similar to that of Na–Cr-rich pyroxene with a less pronounced Ta depletion (Figure 5B). Titanite analyses show convex REE profiles with elevated Ce-Sm (Figure 5A), typical of magmatic titanite (e.g., [30]). Significant Sr and Zr–Hf depletions are also apparent while Nb (but not Ta) is highly enriched.

Chromite shows a heterogeneous major element composition. The analyzed grains mainly differ in the contents of FeO (30.6–51.5 wt %) and Cr_2O_3 (36.1–53.4 wt %; Table 3). All documented chromites are extremely low in magnesium (Mg = 0.01–0.08 apfu-atoms per formula unit; X_{Mg} = 0.58–5.63%). Magnesium contents in chromites are even lower than those of Mn (0.09–0.14 apfu). Titanium and Al are also present in trace amounts (Ti = 0.01–0.02 apfu, Al = 0.02–0.04 apfu). The observed differences most likely reflect significant heterogeneity at a single grain scale, as apparent for Na–Cr-rich pyroxene (Figure 3f), likely also true for other mineral phases.

Table 3. EMPA analyses and structural formulae of chromites from this study.

Sample		IC03F	IC03F	IC03G	IC03G	IC03G
Mineral Phase		Chromite	Chromite	Chromite	Chromite	Chromite
SiO_2		1.17	2.38	0.30	0.09	4.76
TiO_2		0.56	0.21	0.76	0.59	0.63
Al_2O_3		0.67	0.64	0.50	0.39	0.83
Cr_2O_3		48.90	53.36	44.91	36.09	40.64
FeO		37.35	30.61	45.36	51.46	40.48
MnO		4.04	3.47	2.86	2.93	2.48
MgO		0.62	0.47	0.18	0.19	1.26
CaO		0.47	0.74	0.31	0.61	0.48
Na_2O		0.00	0.19	0.00	0.00	0.02
K_2O		0.04	0.07	0.02	0.00	0.07
Total		93.80	92.15	95.23	92.35	91.65
X_{Mg} (mol %)		3.23	2.80	0.68	0.58	5.63
M1	Fe^{2+}	0.84	0.86	0.92	0.91	0.85
	Mn	0.14	0.12	0.09	0.10	0.09
	Mg	0.04	0.03	0.01	0.01	0.08
M2	Fe^{3+}	0.40	0.21	0.55	0.81	0.57
	Cr	1.54	1.75	1.38	1.14	1.35
	Ti	0.02	0.01	0.02	0.02	0.02
	Al	0.03	0.03	0.02	0.02	0.04

All data are in wt %. X_{Mg} is calculated in mol % as 100 × MgO/(MgO + FeO_{tot}). Structural chemical formulae data in apfu (atoms per formula unit) are based on 3 cations and 4 oxygens. The relatively low totals are related to the high amount of ferric iron, analyzed as ferrous iron by the electron microprobe.

5. Discussion and Concluding Remarks

The presence of Na–Cr-rich pyroxene in carbonatites remains somewhat enigmatic. Experimental data of Marušková et al. [31] indicate that kosmochlor is stable at a rather limited range of temperatures between ~950 and ~1100 °C, with the maximum temperature stability at ~1000–1040 °C. Kosmochlor decomposes to eskolaite (Cr_2O_3), silica and sodium silicate above ~1100 °C [31] although eskolaite can also be consumed to form kosmochlor during high-temperature retrograde metamorphism and metasomatism of diopside at 600–700 °C and 5–6 kbar [32], following reaction (1):

$$CaMgSi_2O_6 + Cr_2O_3 + Na^+ = NaCrSi_2O_6 + Ca^{2+} + Mg^{2+} \quad (1)$$

Eskolaite could also be considered as a proxy mineral phase for the presence of kosmochlor and may be present as inclusions in other mineral phases. However, no eskolaite was found in the samples investigated here, which could be the result of its instability in the observed paragenesis owing to Na input via metasomatism (extensive fenitization is known from the Samalpatti complex; e.g., [21]) and resulting formation of Di-Kos solid solution as proposed by Vasil'ev et al. [32], or formation of Cr-rich pyroxene by another process. Eskolaite could also be the source for formation of magnesiochromite as proposed by Reznitsky et al. [2] via the reaction (2):

$$Cr_2O_3 + CaMg(CO_3)_2 = MgCr_2O_4 + CaCO_3 + CO_2 \quad (2)$$

With respect to ferrous rather than magnesian character of the system in Samalpatti, the reaction (2) should be modified to:

$$Cr_2O_3 + CaFe(CO_3)_2 = FeCr_2O_4 + CaCO_3 + CO_2 \quad (3)$$

Shi et al. [33] suggested the formation of Cr-rich pyroxene from primary chromite via its decomposition and incorporation of Cr and Na into pyroxene that can be defined by the following reactions:

$$MgCr_2O_4 \text{ (magnesiochromite)} + 4SiO_2(aq) + 2Na^+(aq) = 2NaCrSi_2O_6 + Mg^{2+}(aq) \quad (4)$$

$$FeCr_2O_4 \text{ (chromite)} + 4SiO_2(aq) + 2Na^+(aq) = 2NaCrSi_2O_6 + Fe^{2+}(aq) \quad (5)$$

$$Fe^{2+}Fe_2{}^{3+}O_4 \text{ (magnetite)} + 4SiO_2(aq) + 2Na^+(aq) = 2NaFeSi_2O_6 \text{ (aegirine)} + Fe^{2+}(aq) \quad (6)$$

$$MgAl_2O_4 \text{ (spinel)} + 4SiO_2(aq) + 2Na^+(aq) = 2NaAlSi_2O_6 \text{ (jadeite)} + Mg^{2+}(aq) \quad (7)$$

Chromite in our samples is generally Mg-poor (<1 wt % MgO; see Section 4.2) and reaction (5) can thus be taken as representative. We believe that sodium is sourced from intruded carbonatites which often are enriched in Na_2O (up to 4.6 wt %; [16]).

Another mechanism of forming Na–Cr-rich pyroxene was proposed by Rosenthal et al. [34] which showed that kosmochlor could be formed in the reaction zone layer (RZL) between eclogitic melt and peridotitic mantle according to the reaction (8) although eclogites have not been reported from the surface geology in the Samalpatti area [22,35].

$$(Ca,Mg)_3(Cr,Fe^{3+})_2Si_3O_{12} + 2NaAlSi_2O_6 = 2Na(Cr,Fe^{3+})Si_2O_6 + (Ca,Mg)_3Al_2Si_3O_{12} \quad (8)$$

$$[Cr\text{-}Fe^{3+} \text{ garnet (peridotite)} + \text{jadeite (eclogitic melt)} = \text{kosmochlor/aegirine} + \text{grossular}] \quad (9)$$

The reactions (1) and (4)–(8) described in the literature suggest the important role of sodic metasomatism of mantle-derived minerals for the formation of Na–Cr-rich pyroxene. To further constrain the possible origin of Na–Cr-rich pyroxene from Samalpatti, we plotted new data from this study in the ternary Kos-Quad-Jd + Ae plot of Ikehata and Arai [27]. While several new analyses plot close to some kimberlites and high-pressure metamorphic rocks, the majority of our data fills previously unoccupied regions in the Kos–Quad-Jd + Ae space (Figure 4B). This indicates that Na–Cr-rich pyroxene in the silicate-carbonatite association from Samalpatti may have a distinct origin and history compared to those reported for other occurrences. We note that alkaline metasomatism (fenitization) is a process commonly associated with carbonatite intrusions [36] and has been evidenced in Tamil Nadu carbonatite occurrences [21].

From mineral chemistry and observed textures, we envisage two possible models.

(1) The Na-Cr-rich pyroxene could have been derived from chromian-rich mantle minerals (chromite and/or garnet) through fenitization related to intrusion of carbonatite melts which provided supply of alkalis, and sodium in particular. Further metasomatism could result in corrosion of Na–Cr-pyroxene and transfer of part of Cr into winchite, which based on petrographic observations and chemistry is late to Na–Cr-rich pyroxene. The origin of winchite by corrosion of Na–Cr-rich pyroxene is supported mainly by its textures, and also by concentrations of incompatible trace elements (Figure 4B), which display patterns resembling that of Na–Cr-rich pyroxene. Chromites in thin-sections are present in form of skeletal aggregates or as inclusions in Na–Cr-rich pyroxenes, which is the result of their decomposition. Chromium from decomposed chromites was first incorporated into Na–Cr-rich pyroxenes and later into winchite. Concentration of Cr in winchite (1700–3500 ppm) is significantly lower than that in Na–Cr-rich pyroxene (up to 118,500 ppm), but winchite is more abundant, consuming a larger portion of available Cr. Titanite was then formed from the excess of Ca and Ti generated during later stages of fenitization. This was possible due to long-lasting magmatic and post-emplacement activity in the Samalpatti complex. Preliminary K–Ar da yielded the ages of 800–700 Ma which is consistent with Moralev et al. [17], but data for syenites appear to yield significantly younger ages at ~570 Ma [37] indicating poly-phase evolution of the Samalpatti complex. Thus, the observed composition of Na–Cr rich pyroxenes points to a possible model,

where chromite- or Cr-rich garnet-bearing peridotite was fenitized in association with emplacement of carbonatite magma. The fenitization produced Na–Cr-rich pyroxene, but further metasomatism (probably polyphase) associated with additional input of volatile species resulted in corrosion of the Na–Cr-rich pyroxene by growing winchite. Such a model, however, has several issues. First, the investigated chromite is Fe-rich (X_{Mg} = 0.2–1.6%). The available literature data on chromites from mantle rocks or mantle-derived melts document relatively wide compositional spectra reflecting variable conditions of origin (e.g., [37–39]). Among these, chromites from forearc peridotites tend to be more Fe-rich but never with X_{Mg} values < 20% [36]. Second, Na–Cr-rich pyroxene shows a wide spectrum of chemistry while magmatic crystallization from a homogeneous batch of mantle magma would likely yield uniform composition of kosmochlor and its solid solutions (Figure 4B). Third, pyroxenes with lower proportions of the kosmochlor end-member are associated with larger and more abundant chromite grains (samples IC03F and IC03G).

(2) Mantle association of olivine + pyroxene and Cr-rich garnet could have been decomposed during percolation of Na-rich carbonatite melt. This could result in formation of kosmochlor–quad solid solution, titanite and calcite, and winchite in a later stage. Whether the garnet would be a Cr-enriched common mantle garnet [$(Mg,Fe^{2+},Ca)_3(Al,Cr)_2(SiO_4)_3$], or even a more pure uvarovite-like garnet [$Ca_3Cr_2(SiO_4)_3$], would remain to be investigated in detail using experimental petrology. For example, Na–Cr-rich pyroxene corroding garnet in peridotite microxenoliths was described from the Zagadochnaya kimberlite and interpreted as a result of melt infiltration into the metasomatized garnet lherzolite [40]. However, pseudomorphs after garnet have not been observed and a source of Ti is also unclear. Moreover, garnet should carry elevated HREE abundances which is not observed in any possible product of its decomposition. In contrast, Ziberna et al. [40] documented significant modification of REE patterns in garnet affected by metasomatism and growth of secondary pyroxene. In addition, the secondary pyroxene grown in garnet in Zagadochnaya kimberlite displays strong LREE enrichment (La_N ~100), ~10× exceeding LREE enrichments observed in Samalpatti Na–Cr-rich pyroxene. We note here, that the Samalpatti suite experienced post-emplacement alteration apparent from shifted C-O stable isotope systematics, which could lead to loss of LREE [16]. Nevertheless, Seyler and Brunelli [41] described that very low LREE/HREE, paralleled by low Ti contents in pyroxene and spinel, are typical for residual peridotites, which is consistent with our hypothesis of peridotite protolith of silicocarbonatites from Samalpatti.

Collectively, the appearance of kosmochlor and Na–Cr-rich pyroxene in general may play an important role in deconvolving metasomatic processes, and fenitization in particular, in the mantle if a systematic endeavour in exploring Cr-rich mantle domains and their reaction haloes is undertaken. This, combined with careful petrologic experiments, could lead to our improved understanding of the origin and history of chemical signatures of carbonate-rich materials in the mantle and their impact on supply, loss and distribution of trace elements.

Supplementary Materials: The following are available online at http://www.mdpi.com/2075-163X/8/8/355/s1, Table S1: Kratky etal_Supplementary table S1 and Kratky etal_Supplementary table S2.

Author Contributions: O.K., V.R. and T.M. designed the study; O.K., V.R. and M.R. performed the EMPA analyses; J.M. and O.K. performed LA-ICPMS analyses; all authors participated in writing the manuscript and data interpretation.

Funding: This study was funded by the Czech Science Foundation project Nr. 15-08583S. We acknowledge partial support from the Czech Geological Survey grant Nr. 310150.

Acknowledgments: We are grateful to Dewashish Upadhyay (IIT Kharagpur) for assistance during the field work, Patricie Halodová (Czech Geological Survey) for help with SEM analyses and Anja Rosenthal (Laboratoire Magmas et Volcans) for discussion.

Conflicts of Interest: The authors declare no conflict of interests.

References

1. Morimoto, N.; Fabries, J.; Ferguson, A.K.; Ginzburg, I.V.; Ross, M.; Seifert, F.A.; Zussman, J.; Aoki, K.; Gottardi, G. Nomenclature of pyroxenes. *Miner. Petrol.* **1988**, *73*, 1123–1133.
2. Reznitsky, L.Z.; Sklyarov, E.; Galuskin, E. Complete isomorphic join diopside–kosmochlor $CaMgSi_2O_6$–$NaCrSi_2O_6$ in metamorphic rocks of the Sludyanka complex (southern Baikal region). *Russ. Geol. Geophys.* **2011**, *52*, 40–51. [CrossRef]
3. Laspeyres, H. Die steinigen Gemengtheile im Meteoreisen von Toluca in Mexico. *Z. für Kryst. Mineral.* **1897**, *27*, 586–600.
4. Frondel, C.; Klein, C., Jr. Ureyite, $NaCr_2Si_2O_6$, a new meteoritic pyroxene. *Science* **1965**, *149*, 742–744. [CrossRef] [PubMed]
5. Couper, A.G.; Hey, M.H.; Hutchison, R. Cosmochlore: A new examination. *Mineral. Mag.* **1981**, *44*, 265–267. [CrossRef]
6. Zinovieva, N.G.; Mitreikina, O.B.; Granovsky, L.B. Matrix Material of the Yamato-74417 Ordinary Chondrite (L3). In Proceedings of the 30th Annual Lunar and Planetary Science Conference, Houston, TX, USA, 15–29 March 1999. Abstract No. 1019.
7. Joswiak, D.J.; Brownlee, D.E.; Matrajt, G.; Westphal, A.J.; Snead, C.J. Kosmochloric Ca-rich pyroxenes and FeO-rich olivines (Kool grains) and associated phases in Stardust tracks and chondritic porous interplanetary dust particles: Possible precursors to FeO-rich type II chondrules in ordinary chondrites. *Meteorit. Planet. Sci.* **2009**, *44*, 1561–1588. [CrossRef]
8. Gainsforth, Z.; Butterworth, A.L.; Stodolna, J.; Westphal, A.J.; Huss, G.R.; Nagashima, K.; Ogliore, R.; Brownlee, D.E.; Joswiak, D.; Tyliszczak, T.; et al. Constraints on the formation environment of two chondrule-like igneous particles from comet 81P/Wild 2. *Meteorit. Planet. Sci.* **2015**, *50*, 976–1004. [CrossRef]
9. Wooden, D.H.; Ishii, H.A.; Zolensky, M.E. Cometary dust: The diversity of primitive refractory grains. *Philos. Trans. R. Soc. A* **2017**, *375*. [CrossRef] [PubMed]
10. Mével, C.; Kiénastr, J.R. Chromian jadeite, phengite, pumpellyite and lawsonite in high-pressure metamorphosed gabbro from the French Alps. *Mineral. Mag.* **1980**, *43*, 979–984. [CrossRef]
11. Yang, C.M.O. A terrestrial source of ureyite. *Am. Mineral.* **1984**, *69*, 1180–1183.
12. Liu, X.C.; Zhou, H.Y.; Ma, Z.S.; Chang, L.H. Chrome-rich clinopyroxene in orthopyroxenite from Maowu, Dabie Mountains, central China: A second record and its implications for petrogenesis. *Isl. Arc* **1998**, *7*, 135–141. [CrossRef]
13. Sobolev, V.N.; Taylor, L.A.; Snyder, G.A.; Sobolev, N.V.; Pokhilenko, N.P.; Kharkiv, A.D. A unique metasomatized peridotite xenolith from the Mir kimberlite pipe (Yakutia). *Geol. Geofiz.* **1997**, *38*, 206–215.
14. Reznitskij, L.Z.; Sklyarov, E.V.; Karmanov, N.S. The first occurrence of kosmochlor (ureyite) in metasediments. *Proc. USSR Acad. Sci.* **1999**, *364*, 523–526.
15. Sobolev, V.S.; Sobolev, N.V.; Lavarnt'eva, U.Y.G. Chrome-rich clinopyroxenes from the kimberlities of Yakutia. *Neues Jahrbuch für Mineralogie* **1975**, *123*, 213–218.
16. Ackerman, L.; Magna, T.; Rapprich, V.; Upadhyay, D.; Krátký, O.; Čejková, O.; Erban, V.; Kochergina, Y.V.; Hrstka, T. Contrasting petrogenesis of temporally related carbonatites from Samalpatti and Sevattur, Tamil Nadu, India. *Lithos* **2017**, *284–285*, 257–275. [CrossRef]
17. Moralev, V.M.; Voronovski, S.N.; Borodin, L.S. New findings about the age of carbonatites and syenites from southern India. *USSR Acad. Sci.* **1975**, *222*, 46–48.
18. Udas, G.R.; Krishnamurthy, P. Carbonatites of Sevathur and Jokipatti, Madras State, India. *Proc. Indian Natl. Sci. Acad.* **1970**, *36*, 331–343.
19. Viladkar, S.G.; Subramanian, V. Mineralogy and geochemistry of the carbonatites of the Sevathur and Samalpatti complexes, Tamil Nadu. *J. Geol. Soc. India* **1995**, *45*, 505–517.
20. Grady, C. Deep main faults in south India. *J. Geol. Soc. India* **1971**, *12*, 52–62.
21. Srivastava, R.K. Petrology of the Proterozoic alkaline carbonatite complex of Samalpatti, district Dharmapuri, Tamil Nadu. *J. Geol. Soc. India* **1998**, *51*, 233–244.
22. Subramanian, V.; Viladkar, S.G.; Upendran, R. Carbonatite alkali complex of Samalpatti, Dharmapuri district, Tamil Nadu. *J. Geol. Soc. India* **1978**, *19*, 206–216.

23. Schleicher, H.; Kramm, U.; Pernicka, E.; Schidlowski, M.; Schmidt, F.; Subramanian, V.; Todt, W.; Viladkar, S.G. Enriched subcontinental upper mantle beneath southern India; evidence from Pb, Nd, Sr and C-O isotopic studies on Tamil Nadu Carbonatites. *J. Petrol.* **1998**, *39*, 1765–1785. [CrossRef]
24. Vieten, K.; Hamm, H.M. Additional notes on the calculation of the crystal chemical formula of clinopyroxenes and their contents of Fe^{3+} from microprobe analyses. *Neues Jahrbuch für Mineralogie* **1978**, *2*, 71–83.
25. Whitney, D.L.; Evans, B.W. Abbreviations for names of rock-forming minerals. *Am. Mineral.* **2010**, *95*, 185–187. [CrossRef]
26. Sakamoto, S.; Takasu, A. Kosmochlor from the Osayama ultramafic body in the Sangun metamorphic belt, southwest Japan. *J. Geol. Soc. Jpn* **1996**, *102*, 49–52. [CrossRef]
27. Ikehata, K.; Arai, S. Metasomatic formation of kosmochlor-bearing diopside in peridotite xenoliths from North Island, New Zealand. *Am. Mineral.* **2004**, *89*, 1396–1404. [CrossRef]
28. Anders, E.; Grevesse, N. Abundances of the elements: Meteoric and solar. *Geochim. Cosmochim. Acta* **1989**, *53*, 197–214. [CrossRef]
29. McDonough, W.F.; Sun, S.-S. The composition of the Earth. *Chem. Geol.* **1995**, *120*, 223–253. [CrossRef]
30. Fu, Y.; Sun, X.M.; Zhou, H.Y.; Lin, H.; Yang, T.J. In-situ LA-ICP-MS U–Pb geochronology and trace elements analysis of polygenetic titanite from the giant Beiya gold–polymetallic deposit in Yunnan Province, Southwest China. *Ore Geol. Rev.* **2016**, *77*, 43–56. [CrossRef]
31. Maruskova, K.; Had, J.; Maryska, M.; Sanda, L.; Hlavac, J. High-temperature reactions of sodium chromate with silica. *Ceram. Silik.* **1997**, *41*, 105–111.
32. Vasil'ev, E.P.; Reznitsky, L.Z.; Vishnyakov, V.N.; Nekrasova, E.A. *The Sludyanka Metamorphic Complex*; Nauka: Novosibirsk, Russia, 1981. (In Russian)
33. Shi, G.H.; Stockhert, B.; Cui, W.Y. Kosmochlor and chromian jadeite aggregates from the Myanmar jadeitite area. *Mineral. Mag.* **2005**, *69*, 1059–1075. [CrossRef]
34. Rosenthal, A.; Yaxley, G.M.; Green, D.H.; Hermann, J.; Kovacs, I.; Spandler, C. Continuous eclogite melting and variable refertilisation in upwelling heterogeneous mantle. *Sci. Rep.* **2014**, *4*, 6099. [CrossRef] [PubMed]
35. Gittins, J. The origin and evolution of carbonatite magmas. In *Carbonatites: Genesis and Evolution*; Bell, K., Ed.; Unwin Hyman Ltd.: London, UK, 1989; pp. 580–600.
36. Lian, D.; Yang, J.; Dilek, Y.; Wu, W.; Zhang, Z.; Xiong, F.; Liu, F.; Zhou, W. Deep mantle origin and ultra-reducing conditions in podiform chromitite: Diamond, moissanite, and other unusual minerals in podiform chromitites from the Pozanti-Karsanti ophiolite, southern Turkey. *Am. Mineral.* **2017**, *102*, 1101–1113.
37. Rapprich, V.; Pécskay, Z.; Magna, T.; Míková, J. Age disparity for spatially related Sevattur and Samalpatti carbonatite complexes. In Proceedings of the Goldschmidt 2017 Conference #3280, Paris, France, 13–18 August 2017.
38. Maibam, B.; Foley, S.; Luguet, A.; Jacob, D.E.; Singh, T.B.; Ray, D.; Panda, D.K.; Keppler, R. Characterisation of chromites, chromite hosted inclusions of silicates and metal alloys in chromitites from the Indo-Myanmar ophiolite belt of Northeastern India. *Ore Geol. Rev.* **2017**, *90*, 260–273. [CrossRef]
39. Latypov, R.; Costin, G.; Chistyakova, S.; Hunt, E.J.; Mukherjee, R.; Naldrett, T. Platinum-bearing chromite layers are caused by pressure reduction during magma ascent. *Nat. Commun.* **2018**, *9*, 462. [CrossRef] [PubMed]
40. Na, L.; Nimis, P.; Zanetti, A.; Sobolev, N.V.; Marzoli, A. Geochemistry of garnets and clinopyroxenes in microxenoliths from the Zagadochnaya kimberlite (Yakutia, Russia). *Plinius* **2010**, *36*, 311.
41. Seyler, M.; Brunelli, D. Sodium chromium covariation in residual clinopyroxenes from abyssal peridotites sampled in the 43°–46° E region of the Southwest Indian Ridge. *Lithos* **2018**, *302*, 142–157. [CrossRef]